Label-free electrochemical immunoprobe for dengue infection marker detection

Mosquito-borne flavivirus dengue infection is the major cause of consecutive epidemics in the tropical and subtropical regions of the world. The World Health Organization has estimated nearly 100–400 million dengue cases every year[1]. Epidemiological study suggests that from 1998 to 2014 there has been high incidence of dengue in Pondicherry (372.92), Dadra Nagar Haveli (176.31) and Delhi (102.15). Likewise, states of Punjab, Gujarat, Karnataka, Kerala, Tamil Nadu and Orissa were reported to have high dengue incidence in the range 21 and 50 per million[2]. Recent data also documented that 110,473 dengue cases were observed in India between January and October 2022. Mild fever to life-threatening dengue hemorrhagic fever (DHF) and dengue shock syndrome (DSS) can cause failure in the circulatory system and liver function[3], which implies a need for rationalized treatments to reduce the mortality rate. Therefore, clinical diagnosis is required to study nucleic acids, virions, serologic or antigenic components of dengue infection[4]. A non-structural 1 (NS1) protein received from dengue-infested cells has been recognized as a predictive marker of DHF[5]. But rapid and selective detection of clinical marker in dengue infection suspected patients especially in decentralized health centres is highly challenging. Thus, there is a need for rationalized diagnosis of the dengue-associated early surrogate marker, i.e. NS1 protein at the point-of-need. The most common methods of clinical diagnosis involve serological test[6], virus isolation[7], detection of viral genomes[8] and antigens[9]. Unlike traditional assays, the electrochemical method has been demonstrated to be field-deployable, user-friendly, highly reliable, sensitive and selective against different varieties of target analytes[10]. Figure 1 illustrates the dengue virus model, viral genome composition and clinical serological survey during dengue infection with *in situ* redox-active electrochemical biosensor platform for specific detection of different analytes.

The development of *in situ* redox-active (label-free) transducer is an important research area under electrochemical biosensors having potential utility for point-of-need analysis[11]. Specifically, immunosensor platforms are highly selective due to their inherent specificity between the antibody and antigen, which could be useful for infectious disease diagnosis[10]. However, analysing the antibody–antigen interaction from a complex biological matrices at the interface of disposable working electrode surface with retained bioaffinity and durable signal transduction is highly challenging. In this context, graphene-derivatives, viz. graphenes oxide (GO) and reduced GO (rGO) nanosheets hybridized with different metals, metal oxides or polymer-based nanocomposites are processed as (bio)sensor platforms due to their unique physico-chemical properties[12].

Recently, we have developed dual-functional graphene oxide–ruthenium bipyridine (GO-Rubpy) nanosheets prepared using the wet-chemical approach, exhibiting optical and redox-active functions as revealed from photoluminescence and voltammetric behaviour[13]. As established GO-Rubpy nanosheets were then processed on carbon screen-printed electrodes with a suitable bioaffinity layer and monoclonal antibodies (mAbs) of NS1 protein to form the electrochemical immunosensor platform. Unlike conventional electrochemical biosensors, GO-Rubpy-modified electrodes enabled *in situ* redox behaviour without any external mediator for immunocomplex formation. Distinct from electrochemical immunoassays, fluorescence-based immunosensing is assisted by the chitosan layer as an additive membrane for better loading of mAbs. Both electrochemical- and optical-based detection exhibited a sub-clinical level of detection of NS1 protein in real serum samples, even in the presence of serum-associated interferents[13].

Figure 2 *a* is a schematic diagram of the fabricated GO-Rubpy/Pro-G/mAb/SPE showing its electrochemical behaviour in the presence and absence of NS1 protein. From the cyclic voltammogram, it can be observed that the GO-Rubpy/Pro-G/mAb electrode (Figure 2 *a* (inset)) exhibits a quasi-reversible behaviour due to the electrochemical conversion of $Ru^{2+} \Leftrightarrow Ru^{3+}$. The noticeable quenching of current density after NS1 protein interaction (top panel sensor surface and CV illustration; Figure 2 *a*) confirms the immune complex formation on the electrode–electrolyte interface, apparently hindering the electron transfer of GO-Rubpy moieties on the electrode surface. Understanding the electrode–electrolyte barrier, especially during the immunocomplex formation, is vital for efficient immunosensor construction. Figure 2 *b* shows the electrochemical impedance spectroscopic (EIS) data of layer-by-layer modified electrode system with the target NS1 protein, using 0.01 M PBS as the supporting electrolyte in the frequency range 0.1–10,000 Hz. From the empirical analysis, the charge transfer resistance (R_{ct}) of
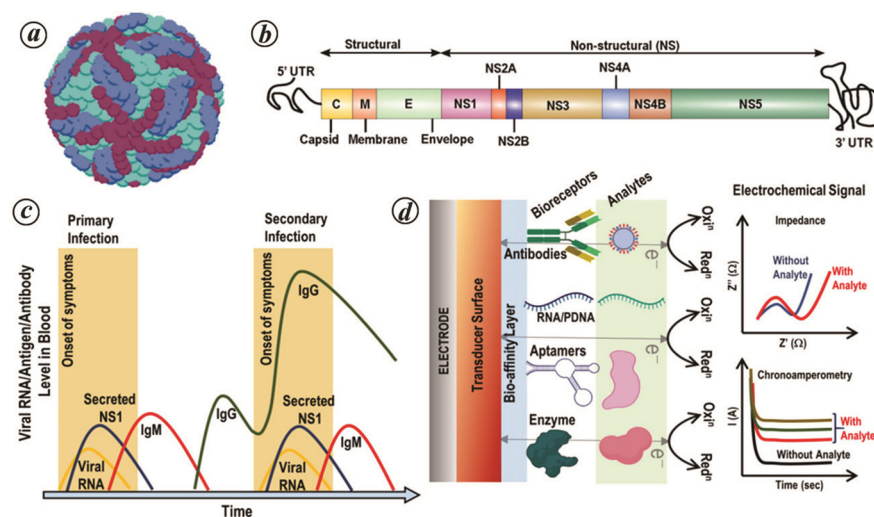

Figure 1. *a*, Structure of the dengue virus. *b*, Dengue viral RNA and its components. *c*, Serological biomarker expression level during dengue infection. *d*, Skeletal representation of biosensor platform with different bioreceptor modifications depicting the *in situ* electrochemical redox (label-free) signal transduction.

GO-Rubpy/SPE with sequential modification of the bioaffinity layer (protein-G), bioreceptor (mAb of NS1) and target NS1 protein were distinguishable, revealing the potential in further clinical diagnosis without any external redox-probe.

To complement EIS, chronoamperometric (CA)-based detection of NS1 protein at a wide range was performed using an oxidation potential of +1.1 V (versus Ag/AgCl) as the bias potential (Figure 3 a). CA current response at 50 sec against dengue antigen was calibrated to determine the linear range of detection (1 ng/ml to 100 µg/ml). The concentration-dependent quenching was clearly observed from the relative his-

tograms between the current (%) and NS1 protein (Figure 3 b). Relative amperometric current (%) for the analyte was calculated using the formula $I_c/I_0 \times 100$. The current observed at GO-Rubpy/Pro-G/mAb/SPE with different concentrations of NS1 protein is represented as I_c: 1 ng/ml to 100 µg/ml, and without NS1 protein is represented as I_0. The selectivity of GO-Rubpy/Pro-G/mAb electrode against the target was validated by introducing serological interferents, viz. immunoglobulin-G, fibrinogen and human serum albumin. Relative histogram of CA results shows that the interferents on the electrode surface have negligible interaction with the mAb NS1-modified GO-Rubpy electrode interface (Figure 3 c).

For field analysis, the as-developed, label-free electrochemical immunosensor platform was tested against human serum (diluted) samples spiked with different concentrations of the target NS1 protein. Serum samples of ten different healthy volunteers were collected from the Health Centre, CSIR-Central Electrochemical Research Institute, Karaikudi, Tamil Nadu, India, following Institutional Safety Ethical Committee guidelines. Chronoamperograms of the fabricated electrochemical immunosensor platform with different pristine serum samples and spiked NS1 protein concentrations were studied. Statistical correlation demonstrates that the diluted serum samples exhibit current density of 60–66 µA/cm², which is in agreement with the blank experiment performed without NS1 protein in 0.01 M PBS[13]. The NS1 protein spiked serum samples exhibit distinguishable decreased current density corresponding to the analyte concentration. Based on the experimental analysis, it can be summarized that the *in situ* redox-active sensor element GO-Rubpy is highly beneficial for point-of-need analysis. The major advantages of this study include cost-efficient synthesis protocol, user-friendly immunosensor construction, durable electrochemical behaviour, and sub-clinical analysis of the dengue-associated marker without external redox mediator.
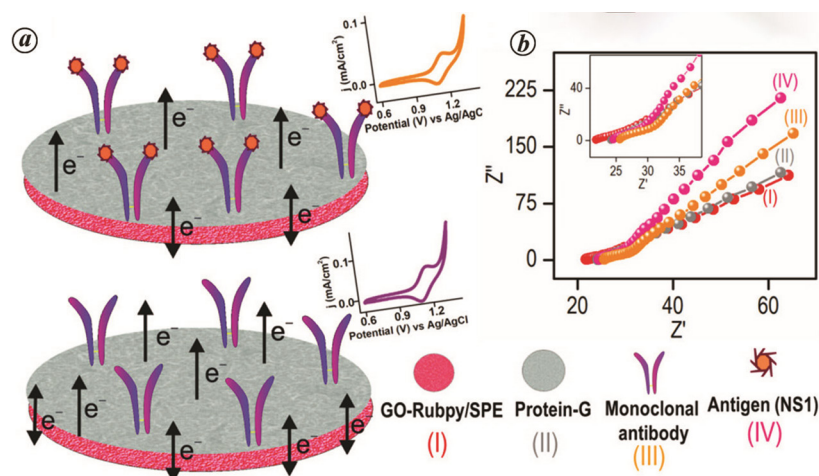

Figure 2. a, Electron transfer mechanism from an *in situ* redox-active electrode surface of GO-Rubpy/SPE immobilized with mAb for NS1 protein detection. b, Electrochemical impedance spectra recorded at layer-by-layer modification of dengue immunosensor platform.
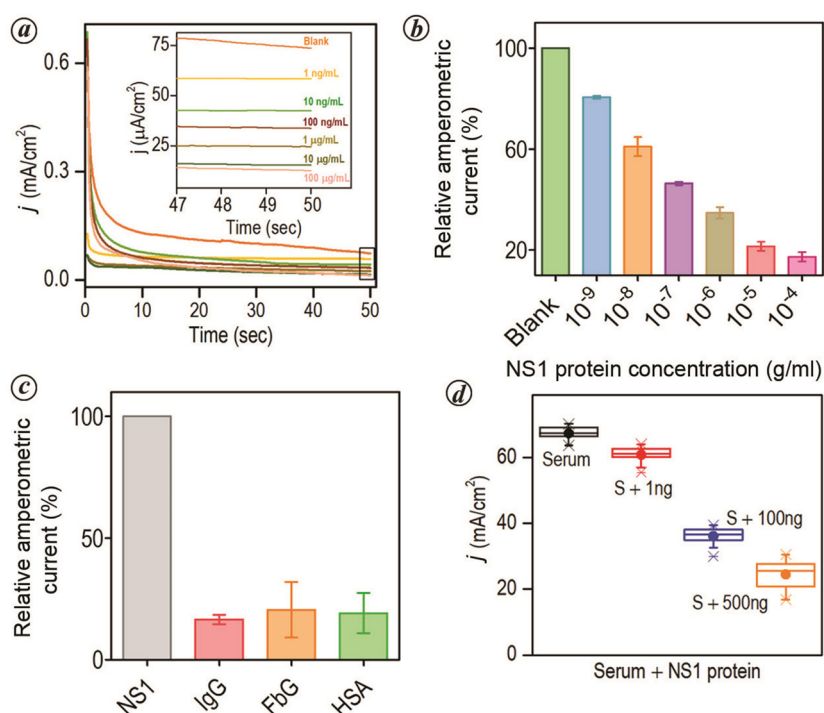

Figure 3. a, Chronoamperometric (CA) response of GO-Rubpy/Pro-G/mAb/SPE versus different concentrations of NS1 protein. Enlarged view of current density response up to 50 sec. b, Histogram obtained from CA results. c, Relative histogram depicting the current observed from GO-Rubpy/Pro-G/mAb-modified electrode against target NS1 protein and interferents separately modified on the electrode surface. d, Statistical analysis of CA response of ten different serum samples spiked with NS1 protein, performed using one-way ANOVA ($P < 0.001$).

1. https://www.who.int/news-room/fact-sheets/detail/dengue-and-severe-dengue#.YVBe-GzyMQEg.google (accessed on 11 October 2021).
2. Mutheneni, S. R., Morse, A. P., Caminade, C. and Upadhyayula, S. M., *Emerg. Microbes Infect.*, 2017, **6**, 1–10.
3. Chakravarti, A., Matlani, M., Kashyap, B. and Kumar, A., *Indian J. Med. Microbiol.*, 2012, **30**, 222–226.

4. Anusha, J. R., Kim, B. C., Yu, K. H. and Raj, C. J., *Biosens. Bioelectron.*, 2019, **142**, 111511.

5. Lapphra, K. *et al.*, *Diagn. Microbiol. Infect. Dis.*, 2008, **60**, 387–391.

6. Kong, Y. Y., Thay, C. H., Tin, T. C. and Devi, S., *J. Virol. Method.*, 2006, **138**, 123–130.

7. Parkash, O. and Shueb, R. H., *Viruses*, 2015, **7**, 5410–5427.

8. Kim, J.-G., Baek, S. H., Kim, S., Kim, H. I., Lee, S. W., Kailasa, S. K. and Park, T. J., *Talanta*, 2018, **190**, 391–396.

9. Darwish, N. T., Sekaran, S. D., Alias, Y. and Khor, S. M., *J. Pharm. Biomed. Anal.*, 2018, **149**, 591–602.

10. Felix, F. S. and Angnes, L., *Biosens. Bioelectron.*, 2018, **102**, 470–478.

11. Kanagavalli, P., Andrew, C., Veerapandian, M. and Jayakumar, M., *Trends Anal. Chem.*, 2021, 116413.

12. Szunerits, S. and Boukherroub, R., *Interface Focus*, 2018, **8**, 20160132.

13. Kanagavalli, P. and Veerapandian, M., *Biosens. Bioelectron.*, 2020, **150**, 111878.

PANDIYARAJ KANAGAVALLI
MURUGAN VEERAPANDIAN*

*Electrodics and Electrocatalysis Division, CSIR-Central Electrochemical Research Institute,
Karaikudi 630 003, India; and
Academy of Scientific and Innovative Research,
Ghaziabad 201 002, India*
*For correspondence.
e-mail: vmurugan@cecri.res.in

Machine learning-based approach on PRISMA data for mapping Nidar ophiolites in Ladakh, India

Classification of minerals based on spectral signatures from satellite-based hyperspectral sensors is crucial for understanding the geology of a region. Machine learning (ML) techniques have proven to perform flawlessly in remote sensing, as they reduce tedious human efforts by automating calculations. Further, ML helps to distinguish various classes, irrespective of noise present in the data. In the present study, we employed ML-based classification techniques on hyperspectral data from the recently launched (March 2019) PRISMA (PRecursore IperSpettrale della Missione Applicativa) mission by the Italian Space Agency (ASI, Rome, Italy), to assess their accuracy in the lithological mapping of ophiolites. These are a distinct variety of igneous rock assemblages comprising ultramafic, mafic and volcanic lithology representing fragments of oceanic crust and the underlying mantle[1]. With diverse mineralogy and sampling of the mantle, ophiolites are known for hosting high-temperature and pressure minerals, including economically important diamonds and chromites, and serve as excellent probes to study the deep-mantle processes[1]. Further, the association of ophiolites with collisional orogenic belts provides significant information about major tectonic events on Earth.

This study classifies the major lithounits present in the Nidar ophiolite complex, which is exposed towards the southeast of Ladakh, India (32°45′–33°35′N and 78°–79°E). Geologically, the ophiolite sequences at Nidar lie between the metamorphics of the Tso Morari Complex (TMC) in the south and sedimentaries of the Indus and Kargil formations to the north. They start with ultramafic rocks (spinel-bearing dunite, peridotite and pyroxenite veins) at the base, followed by mafic (massive to layered gabbro) in the middle (mantle section) and volcano-sedimentary assemblage (basaltic flows, conglomerates, shale, chert, siltstone and jasperite; crustal section) on the top[2,3]. The molasse sediments of the Indus and Kargil formations are sedimentary in composition, composed of continental shale, grit, conglomerates, sandstone and limestone, and overlain by the Ladakh Batholith with composition essentially of granites and granodiorites[4]. The southern portion of the Nidar ophiolites is associated with Zildat ophiolite melanges (ZOM), which are volcanogenic, and further south, there are metamorphics of TMC[5,6]. Figure 1 *a* shows the geological map of the Nidar ophiolites section[1]. The clastic rocks derived from the adjacent sections are common in all the lithological units distributed by parallel streams cutting the complex and joining the Indus towards the north.

For remote sensing of ophiolites, the dominant mineral phases for ultramafic and mafic lithology include olivine, pyroxene, chromite, spinel and plagioclase, while for sedimentary and associated granites, they are quartz, K-feldspar, calcite, dolomite. The altered rocks formed from weathering include serpentine, carbonates, iron oxides, clay minerals and hydroxides. All these primary and secondary phases are recognized by their diagnostic absorption features in the visible and near-infrared region (VNIR) arising due to electronic transition and vibrations[7] (Table 1). There is a tremendous scope to study these assemblages using high-resolution remote sensing, and when combined with ML classifiers, the results are closer to the ground truth. While considering a large number of classes with similar spectral characteristics, traditional classification techniques have limitations. Classical methods work on a static mathematical model, require human intervention and cannot handle noisy data easily. ML-based classification techniques have been proven to do away with these constraints. The present classification based on mineral composition has used ML algorithms, namely artificial neural network (ANN), extreme gradient boosting (XGBoost), random forest (RF) and support vector machine (SVM). They have been applied to one of the hyperspectral data image tiles of the PRISMA sensor available for the study region. PRISMA provides free hyperspectral imaging data at 30m spatial resolution in 239 bands in the visible, near and short-wave infrared region (400–2500 nm) with 12 nm spectral resolution and 30 km swath coverage[8]. The downloaded level-2 reflectance product (L2D) of the PRISMA data tile was georeferenced and layer-stacked in ENVI®. After processing for noise removal and